



Key factors improving oxygen reduction reaction activity in cobalt nanoparticles modified carbon nanotubes

Atsushi Gabe ^a, Jaime García-Aguilar ^a, Ángel Berenguer-Murcia ^a, Emilia Morallón ^b, Diego Cazorla-Amorós ^{a,*}

^a Departamento de Química Inorgánica and Instituto de Materiales. Universidad de Alicante, Ap. 99, 03080, Alicante, Spain

^b Departamento de Química Física and Instituto de Materiales. Universidad de Alicante, Ap. 99, 03080, Alicante, Spain



ARTICLE INFO

Article history:

Received 9 March 2017

Received in revised form 26 May 2017

Accepted 31 May 2017

Available online 3 June 2017

Keywords:

Oxygen reduction reaction

Electrocatalyst

CoOx nanoparticles

Carbon nanotubes

C–N–Co interaction

ABSTRACT

Multiwall carbon nanotubes (CNTs) decorated with cobalt oxide (CoO_x) nanoparticles (NPs) are prepared in various synthesis conditions to investigate their capability as oxygen reduction reaction (ORR) catalysts for fuel cells in alkaline media. The synthesis conditions include the use of protecting, reducing or complexing agents and heat treatment. Higher ORR activity is possible for smaller size of Co NPs catalysts due to the enlarged interfaces between Co species and CNTs. The addition of polyvinylpyrrolidone (PVP) as protecting agent and NaBH_4 during the preparation procedure is necessary for obtaining the highest activity since it favors the formation of lower oxidation states for Co species and the incorporation of N groups which improve ORR activity. CNTs loaded with only 1 wt.% of Co NPs prepared by a facile method using PVP, NaBH_4 and subsequent heat treatment at 500 °C under N_2 atmosphere, demonstrates both similar catalytic activity and stability than Pt/Vulcan (20 wt.% Pt on Vulcan). The synergic chemical coupling effects between CNTs and CoO_x NPs and the presence of carbon material with pyridinic N and quaternary N groups formed from the protecting agent decomposition, seem to be the main factors responsible for the remarkable electrocatalytic activity.

© 2017 Elsevier B.V. All rights reserved.

1. Introduction

Fuel cells (FCs) are electrochemical devices which transform directly the heat of combustion of a fuel (hydrogen, natural gas, methanol, ethanol, hydrocarbons, etc.) into electricity. The fuel is oxidized electrochemically at the anode, without producing any pollutants (only water and/or carbon dioxide are rejected in the atmosphere), whereas the oxidant (oxygen from the air) is reduced at the cathode. For instance, Alkaline Fuel Cells (AFCs) work with pure hydrogen and oxygen from room temperature to 80 °C. Alkaline electrolytes such as KOH used in AFCs (usually in concentrations of 30–45 wt.%) have an advantage over acidic fuel cells, i.e., the oxygen reduction kinetics is much faster than in acidic media [1]. The power output and lifetime of FCs are directly linked to the behavior of the cathode, where most of the polarization losses occur, because the oxygen reduction reaction (ORR) is a slow reaction compared to the hydrogen oxidation at the anode. As a consequence, cathode development requires special attention to find

the best catalyst and electrode structure to combine performance and stability [2,3]. Platinum (Pt) is the most commonly used and active electrocatalyst for the ORR and all of the Pt-group metals reduce oxygen in alkaline media according to the direct 4-electron process [3]. However, their large-scale commercial application has been precluded due to high cost of Pt. In addition, the Pt-based electrodes suffer from low selectivity to ORR in the presence of other reactions (e.g., methanol oxidation derived from fuel crossover in FCs) and CO deactivation [2,4–6].

In contrast, the inherently faster kinetics of the ORR in alkaline media permits the use of non-noble metal catalysts as cathode electrodes [7,8]. In this sense, a wide range of catalysts including non-noble metals has been explored to replace the Pt-based cathode catalyst [3]. Indeed, metal-free heteroatom-doped carbon materials (N, S, P, B and F), transition metal oxides (e.g., CoO , Co_3O_4 , Cu_2O , MnO_2) and metal nitrogen complexes (Co-N_x , Fe-N_x) on carbon nanomaterials can be promising candidates as non-precious metal catalysts [9–12].

Although transition metal oxides can be good materials for this application, unsupported metal oxide particles do not show a good performance at more negative potentials due to the poor transfer of substrate (O_2) and products (H_2O) [13], making necessary the

* Corresponding author.

E-mail address: cazorla@ua.es (D. Cazorla-Amorós).

synthesis of nanoparticles (NPs) supported on an adequate support like carbon materials. Carbon materials or nanomaterials are useful supports for non-noble metal-based systems, especially for those with low electrical conductivity. Furthermore, the carbon support can provide paths for the flow of electrons in the electrocatalytic system [14]. In this sense, new nanostructured carbon materials such as graphene and carbon nanotubes [15] have widely contributed to deriving advanced electrocatalysts due to their desirable electrical and mechanical properties as well as large surface area.

As non-noble metal catalyst, CoO_x (cobalt oxide)-based carbon catalysts are expected to be one of the promising alternatives to Pt-based electrocatalysts [16,17]. CoO_x supported on graphene and other carbon materials has been reported as highly active electrocatalysts for the ORR [13,18,19]. In order to improve the ORR catalytic activity and stability, some works have focused their research on CoO_x doped with N; for this reason various nitrogen containing ligands were used as precursors to form Co-complexes [20–22]. Liang et al. reported that NPs size of Co_3O_4 (~70 wt.%) grown on nitrogen doped reduced graphene oxide (4–8 nm in size) were smaller than those grown on reduced graphene oxide without nitrogen doping (12–25 nm in size). While the pure Co_3O_4 or reduced graphene oxide alone have a very low catalytic activity, the hybrid material with smaller NPs exhibited an unexpectedly high ORR activity that was further enhanced by nitrogen doping of graphene [21]. Another example was proposed by Yuan et al. where a novel nanowire-structured polypyrrole-cobalt composite was successfully synthesized using cetyltrimethylammonium bromide as surfactant [23]. This electrocatalyst showed a superior ORR performance than that of granular polypyrrole-cobalt catalyst prepared without the surfactant and also a better durability than the commercial 20 wt.% Pt/C catalyst. The high quantity of Co-pyridinic-N groups, which worked as ORR active sites, and its large specific surface area facilitated its ORR activity enhancement. Liu et al. investigated about the dependence of ORR activity on particle size of cobalt monoxides (CoO) and carbon composites [24]. Liu et al. prepared catalysts based on CoO (7 wt.%) supported on Vulcan, with an average size of 3.5, 4.9 and 6.5 nm, using a facile colloidal method avoiding any surfactants of long chain. It was concluded that the ORR activity is enhanced by the smaller CoO NPs due to enlarged interfaces between CoO and carbon materials [24].

Different oxidized phases of Co catalysts were prepared and their ORR activity were characterized by Liang et al. [25]. Composites of CoO 40 wt.% on nitrogen doped carbon nanotube (NCNT) were obtained by thermal annealing of a mixture of $\text{Co}(\text{OAc})_2$ and carbon nanotube at 400 °C in NH_3/Ar atmosphere. Additionally, composites of $\text{Co}_3\text{O}_4/\text{NCNT}$ and CoO_x/NCNT were also prepared by heat treatment in hydrothermal and Ar atmosphere, respectively. Among them, the CoO/NCNT hybrid showed higher ORR current density than $\text{Co}_3\text{O}_4/\text{NCNT}$ and CoO_x/NCNT hybrids due to the strong interaction between the cobalt oxide and carbon material [25]. Uhlig et al. prepared three plasma-treated (300, 450 or 600 W for 120 min) CoO_x catalysts supported on Vulcan containing ~20 wt.% of cobalt with a relatively homogeneous dispersion. Higher ORR activity was confirmed when using higher plasma treatment in KOH and K_2CO_3 electrolytes [26].

In summary, a variety of synthetic methods, conditions and carbon supports for Co modified carbon electrocatalysts have been explored for ORR. In this work, Multiwall carbon nanotubes (CNTs) loaded with different contents of Co NPs were prepared by a facile synthesis method consisting in a mixture of CNTs, a surfactant, a metal precursor (cobalt nitrate) and a reducing agent followed by their pyrolysis. Since the preparation method is able to determine the practicability and performance of electrocatalysts [10], several conditions were investigated to elucidate the relationships between properties of CoO_x , such as amount of CoO_x , NPs sizes, chemical composition and oxidation states of Co and ORR activi-

ties. Finally, a simple synthesis procedure of CoO_x NPs supported on CNTs that achieved high ORR catalytic activity with only 1 wt.% of Co NP is presented and insights into the factors governing the high catalytic activity are discussed.

2. Experimental section

2.1. Preparation of CNTs

CNTs were purchased from Cheap Tubes Inc. (Brattleboro, Vt, USA) with a 95% of purity, outer diameter < 8 nm, length: 10–30 μm and a BET surface area of $484 \text{ m}^2 \text{ g}^{-1}$. Since some metal impurities can be present in the carbon material due to their synthetic procedure and they can affect the electrocatalyst activity [27,28], a purification treatment was performed to remove these impurities. The CNTs were purified by 1 M hydrochloric acid solution for more than 12 h (overnight) at room temperature followed by filtration and washing with distilled water. After the acidic treatment, the CNTs were treated with 6 M sodium hydroxide for 6 h at 50 °C to remove the residual ash content. The resulting CNTs were filtered and washed several times by distilled water until the pH of the filtrate was the same as that of the distilled water. Finally the material was dried at 120 °C.

2.2. Decorating CoO_x nanoparticles on CNTs

For the preparation of the CoO_x -based CNTs materials, the following procedure was used. The necessary amount of Co precursor (cobalt(II) nitrate hexahydrate ($\text{Co}(\text{NO}_3)_2 \cdot 6 \text{ H}_2\text{O}$), Sigma-Aldrich) was dissolved in ethanol for a final nominal metal loading of 1, 9, and 17 wt.% of Co. Together with the Co precursor, the required amount of polyvinylpyrrolidone (PVP 40T, Sigma-Aldrich) were added to obtain a PVP/Co molar ratio of 10. After 2 h under vigorous stirring, the purified CNTs were added to the solution. To favor the CNTs dispersion, the suspension was sonicated for 30 s using an ultrasound probe (Bandelin Sonoplus GM2200, 200 W) at 25% output power. Afterwards, the suspension was stirred for 2 h. The same sonication treatment was repeated before the addition of the reducing agent, sodium borohydride (NaBH_4 , Sigma-Aldrich) at 0 °C in an ice-bath. To ensure the total reduction of the Co(II), the suspension was stirred during 2 h at 0 °C followed by filtering and washing with ethanol. The prepared Co-based CNTs were dried at 80 °C overnight. Finally, the obtained Co decorated CNTs were heat treated at 500 °C under N_2 atmosphere for 1 h to remove PVP [29]. In this study, the Co-based catalysts were named as CNT_Co_1%_500, in reference to the samples prepared with a nominal metal loading of 1 wt.% and treated under N_2 at 500 °C during 1 h. Some catalysts were tested without the N_2 heat treatment at 500 °C. For comparison purposes, additional Co-based CNTs were prepared modifying the described synthesis. One sample was prepared with a nominal metal loading of 1 wt.% without the presence of PVP during the reduction step of the Co precursor. Furthermore, one sample was prepared without using the Co precursor but in the presence of PVP (CNT_PVP_500 sample). The nomenclature used for these samples are CNT_Co_1%_noPVP_500 and CNT_PVP_500, respectively. Moreover, another sample was prepared changing from the reduction agent (NaBH_4) to an ammonia solution (NH_4OH , 0.8 ml of 25 wt.%) to increase the pH and produce the precipitation of the Co oxides/hydroxides, as in a related work [24]. This sample is labeled as CNT_Co_1%_NH₃_500.

2.3. Characterization and electrochemical measurements

Transmission electron microscopy (TEM) images of the materials were taken with a JEOL JEM-2010 microscope operated at

200 kV. The samples were suspended in ethanol to obtain a homogeneous dispersion before drop-casting them on a copper grid and then placed in the measurement chamber. The amount of introduced CoO_x into the CNTs was examined by inductively coupled plasma-optical emission spectroscopy (ICP-OES). The ICP-OES results were obtained using a PerkinElmer Optima 4300 system. The samples were dissolved in 2 ml of concentrated aqua regia and filtered. The solutions were adjusted to a final Co concentration between 0 and 20 ppm for its determination in the linear signal range. The surface composition of the catalysts was investigated by using X-ray photoelectron spectroscopy (XPS) in a K-Alpha of Thermo-Scientific spectrometer, equipped with an Al anode. Elemental analysis of the surfaces was calculated from the areas under the main peak of each atom. Deconvolution of the XPS were done by least squares fitting using Gaussian-Lorentzian curves, and as the background determination, a Shirley line was used. X-ray diffraction (XRD) measurements were performed using Cu K α radiation on a Bruker D8 Advance diffractometer.

Electrochemical activity tests towards ORR were carried out in a three-electrode cell using 0.1 M KOH electrolyte, a Pt wire as counter electrode and Reversible Hydrogen Electrode (RHE) electrode as reference electrode. A rotating ring-disk electrode (RRDE, Pine Research Instruments, USA) equipped with a glassy carbon (GC) disk (5.61 mm diameter) and an attached Pt ring was used as working electrode. The catalysts were dispersed in a solution of 75 vol.% of isopropanol, 25 vol.% of water and 0.02 vol.% of Nafion[®] to prepare a final dispersion of 1 mg/ml of the CoO_x -CNTs material. Typically, 100 μl (mass of electrode is 400 $\mu\text{g}/\text{cm}^2$) of the dispersion was pipetted on a GC electrode to obtain uniform catalysts layer for ORR study although the effect of the mass of electrode (80, 800 and 1600 $\mu\text{g}/\text{cm}^2$) was also studied. The sample on the GC was dried by heating lamp for evaporation of the solvent. Cyclic Voltammetry (CV) and linear sweep voltammetry (LSV) were carried out from 0 to 1 V (vs. RHE). The CV was performed in both N_2 and O_2 saturated atmosphere at 50 mVs^{-1} . The LSV was done in an O_2 -saturated atmosphere for different rotation rates of 400, 625, 900, 1025, 1600 and 2025 rpm at 5 mVs^{-1} . The potential of the ring was kept at 1.5 V (vs. RHE) and the ring current by H_2O_2 oxidation was also measured during the LSV measurement. The electron transfer number (n) of ORR on the catalysts modified electrode was determined by the following equation [30].

$$n = \frac{4 \times Id}{Id + Ir/N} \quad (1)$$

where Id is disk current, Ir is ring current, and N is the collection efficiency of the ring which was experimentally determined to be 0.37.

3. Results and discussion

3.1. Chemical characterization

Table 1 shows the Co content in the prepared catalysts determined by ICP-OES analysis. These results reveal that CoO_x loading on CNTs was successful and samples with sufficiently different Co

Table 1

Composition of Co content calculated of CNT (purified CNTs), CNT_{Co.1%}500, CNT_{Co.9%}500 and CNT_{Co.17%}500.

Sample	Co content/wt.%
CNT	0
CNT _{Co.1%} 500	1.0
CNT _{Co.9%} 500	4.7
CNT _{Co.17%} 500	8.2

contents were prepared. However, the amount of Co obtained for the highest Co contents were lower than the intended values probably due to the lack of adequate interaction between the CNTs surfaces and the Co NPs reactants or the limited surface area of CNTs. In this study, we will maintain in the nomenclature the nominal content of Co although the results, if necessary, will be referred to the real Co content of the catalysts.

Table 2 shows nitrogen atomic composition obtained from XPS (XPS survey spectra and C, N and O atomic compositions for prepared catalysts are shown in Fig. S1 and Table S1, respectively). The catalysts prepared with PVP presents a detectable nitrogen content while for CNT and CNT_{Co.1%}noPVP_500 nitrogen was not detected. This is because PVP decomposition during catalyst pre-treatment may produce some carbon material which introduces some N doping near Co atoms since PVP molecules are initially coordinating Co atoms on the NPs surface. Specifically, the catalysts prepared with NaBH₄ reveal a relatively higher amount of nitrogen than that prepared with NH₃ (**Table 2**).

Fig. 1 represents the high-resolution Co 2p and N 1s XPS spectra for a selection of CoO_x decorated catalysts. The two peaks at binding energies (BE) around 780 eV and 795 eV are related to Co 2p(3/2) and Co 2p(1/2), respectively [31]. Although the Co(II) and Co(III) sites have similar 2p BE, they can be differentiated when Co_3O_4 species are formed. The BE of Co(II) is found to be at 781.3 eV for Co 2p(3/2) and 797.3 eV for Co 2p(1/2), whereas the BE of Co(III) is at around 780.0 eV for Co 2p(3/2) and 795.1 eV for Co 2p(1/2) [13,31]. The deconvolution profiles in **Fig. 1** show that the oxidation state of Co on the catalysts prepared herein was mainly Co(II). **Fig. 1a** contains well defined Co(II) peaks for Co 2p(3/2) as well as Co 2p(1/2) for catalysts CNT_{Co.1%}500, CNT_{Co.9%}500 and CNT_{Co.17%}500. In addition, strong satellite peaks at around 785.5 and 804.2 eV presenting 6 eV above the primary spin-orbit BE were observed. These peaks reveal another proof for high-spin Co(II) species [10,32]. Moreover, Co metallic peak at around BE of 778 eV and 793.3 eV were detected for CNT_{Co.1%}500, CNT_{Co.9%}500 and CNT_{Co.17%}500 catalysts [33,34]. In contrast, as shown in **Fig. 1b**, no clear Co 2p peaks, especially for Co 2p(1/2), are observed for 1 wt.% of Co-containing catalyst synthesized without PVP followed by heat-treatment (CNT_{Co.1%}noPVP_500). Interestingly, metallic Co was not detected for CNT_{Co.1%}NH₃500 but the XPS suggests the presence of Co(III) species. In summary, XPS shows that in the synthesis method in which PVP and the reducing agent are used, most of the Co remains as Co(II) together with small amounts of metallic Co. If the reducing agent is not used, Co(III) species are detected. **Fig. S2** shows the XRD patterns of CNT, CNT_{Co.1%}500, CNT_{Co.9%}500, CNT_{Co.17%}500 and

Table 2

N atomic composition obtained from XPS and content of different N species for CNT, CNT_{Co.1%}500, CNT_{Co.9%}500, CNT_{Co.17%}500, CNT_{Co.1%}NH₃500 and CNT_{Co.1%}noPVP_500.

Sample	N/at.%	Quaternary N/%	Pyrrolic/pyridonic N/%	Pyridinic N/%
CNT	0	–	–	–
CNT _{Co.1%} 500	0.77	24.8	30.0	45.2
CNT _{Co.9%} 500	0.77	26.8	30.3	42.9
CNT _{Co.17%} 500	0.99	24.4	31.9	43.7
CNT _{Co.1%} NH ₃ 500	0.28	17.1	53.5	29.4
CNT _{Co.1%} noPVP_500	0	–	–	–

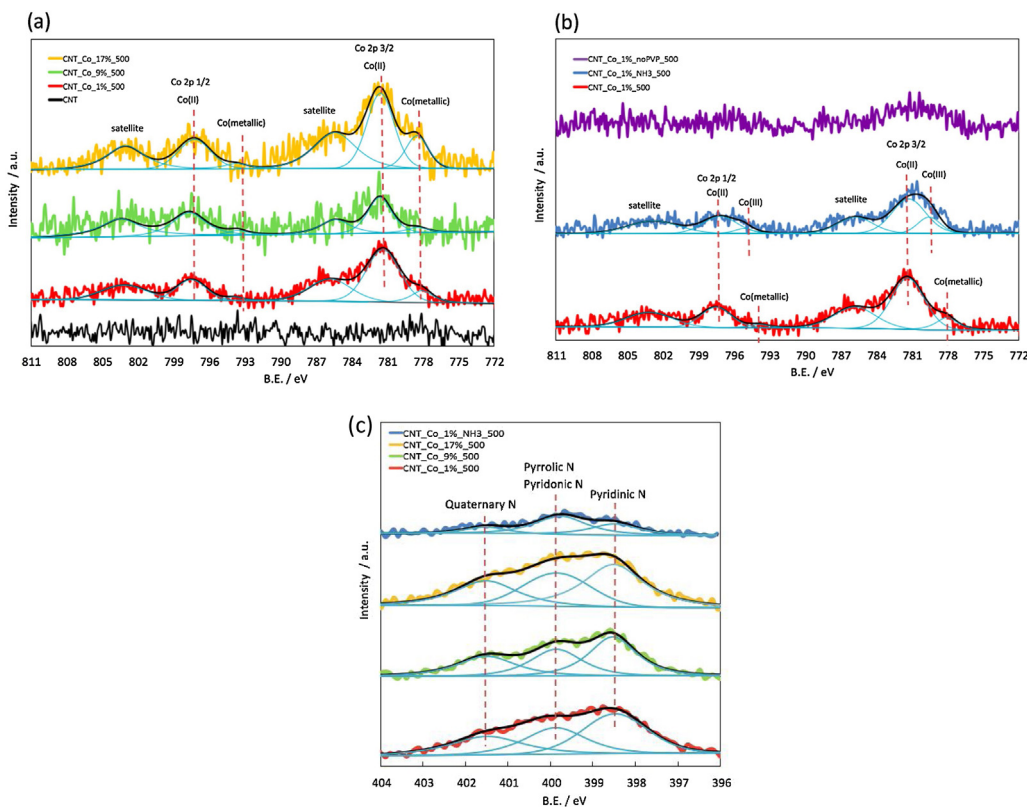


Fig. 1. Co 2p spectra of (a) CNT, CNT-Co_1%, 500, CNT-Co_9%, 500 and CNT-Co_17%, 500 (b) CNT-Co_1%, 500, CNT-Co_1%, NH3, 500 and CNT-Co_1%, noPVP, 500. (c) N 1s spectra of CNT-Co_1%, 500, CNT-Co_9%, 500, CNT-Co_17%, 500 and CNT-Co_1%, NH3, 500.

CNT-Co_1%, NH3, 500. CNT-Co_9%, 500 and CNT-Co_17%, 500. Peaks associated to CoO and Co are only barely observable for the samples with the highest Co content, indicating the existence of both CoO and Co species in these catalysts. However, for the samples with the lowest Co content (CNT-Co_1%, 500 and CNT-Co_1%, NH3, 500) no clear features are distinguished due to the low amount of Co and the small particle size.

Fig. 1c includes the high resolution XPS spectra for N 1s of CNT, CNT-Co_1%, noPVP, 500, CNT-Co_1%, 500, CNT-Co_9%, 500, CNT-Co_17%, 500 and CNT-Co_1%, NH3, 500. The spectra of CNT-Co_1%, 500, CNT-Co_9%, 500, CNT-Co_17%, 500 and CNT-Co_1%, NH3, 500 could be deconvoluted into three peaks with maxima at 398.5, 399.8 and 401.5 eV which indicate pyridinic N, pyrrolic/pyridonic N and quaternary N, respectively [12,23,35,36]. The content of different N species for the catalysts are also indicated in Table 2. Larger N content and more pyridinic N and quaternary N species were detected in samples CNT-Co_1%, 500, CNT-Co_9%, 500 and CNT-Co_17%, 500 than CNT-Co_1%, NH3, 500. To sum up, the preparation protocol using NaBH₄ favors the formation of pyridinic N and quaternary N groups as well as a higher amount of nitrogen content.

Fig. 2 shows the TEM images for catalysts with different amounts of Co but prepared with the same method (CNT-Co_1%, 500, CNT-Co_9%, 500 and CNT-Co_17%, 500) and 1 wt.% of Co-containing catalysts prepared by different synthesis methods (CNT-Co_1%, noPVP, 500 and CNT-Co_1%, NH3, 500). About 100 particles are randomly selected for the analysis of Co_x NPs size distributions. Average NPs size increases with increasing Co content following the same preparation method. However, it remains nearly constant when 1 wt.% of Co is loaded using different preparation methods. These TEM results indicate that the concentration of Co in the catalysts has a greater contribution in the particle size of Co NPs than the chemical agents used in the synthesis. In addition,

Fig. 2f represents high resolution TEM image of CNT-Co_17%, 500 as an example of the prepared catalysts using PVP and NaBH₄. As shown in Fig. 2f, a thin deposit is observed around the Co_x NPs which could be due to the PVP carbonization which may contain most of the N species detected.

3.2. Electrochemical characterization

The ORR catalytic activity of the Co-containing samples was preliminary characterized by CV under N₂ and O₂ saturated atmosphere in 0.1 M KOH. The CV curves for CNT, CNT-Co_1%, 500 and CNT-Co_17%, 500 in N₂ and O₂ saturated atmosphere are shown in Fig. 3a–c respectively. The oxidation current observed for CNT-Co_17%, 500 at potentials higher than 0.8 V vs RHE (Fig. 3c), can be associated to the oxidation of Co(II) to Co(III) according to the following reaction: 3Co²⁺ + 8OH⁻ → Co₃O₄ + 4H₂O + 2e⁻ [25,37]. This oxidation current is not clearly observed for sample CNT-Co_1%, 500 due to the low Co content. The CV curves in Fig. 3b in presence of O₂ show the reduction peak for O₂, which has a more positive onset potential for CNT-Co_1%, 500 and CNT-Co_17%, 500 than CNT. Moreover, the CNT-Co_1%, 500 sample exhibits much higher reduction current than CNT-Co_17%, 500.

To quantitatively investigate the ORR performance, experiments with a RRDE were performed. Fig. 4 represents LSVs and current during ORR for disk and ring electrodes at different rotating rates on CNT and CNT-Co_1%, 500 catalysts. The Limiting Current (LC) increased with increasing the rotating rate due to shortened diffusion distance at high rotating rate [20]. CNT-Co_1%, 500 showed wide current plateau and much higher LC as well as onset potential compared to CNT. These results imply that the addition of Co_x can significantly enhance the ORR activity. Similarly, the measured ring current which corresponds to the oxidation of hydrogen peroxide produced during the LSV curves in the disk electrode (divided

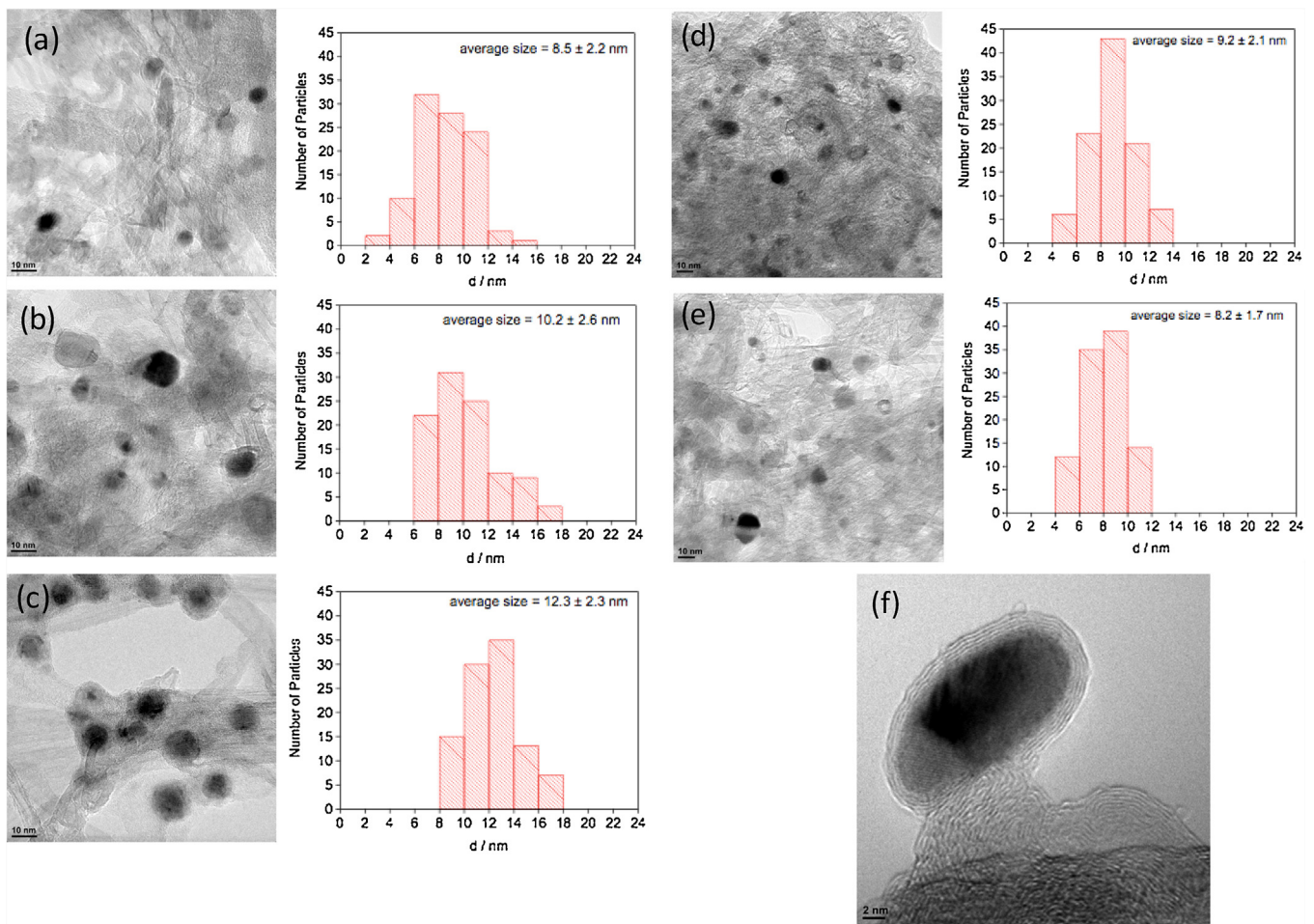


Fig. 2. TEM images of (a) CNT.Co.1%.500, (b) CNT.Co.9%.500, (c) CNT.Co.17%.500, (d) CNT.Co.1%.noPVP.500 and (e) CNT.Co.1%.NH3.500. TEM image of (f) CNT.Co.17%.500 with high resolution.

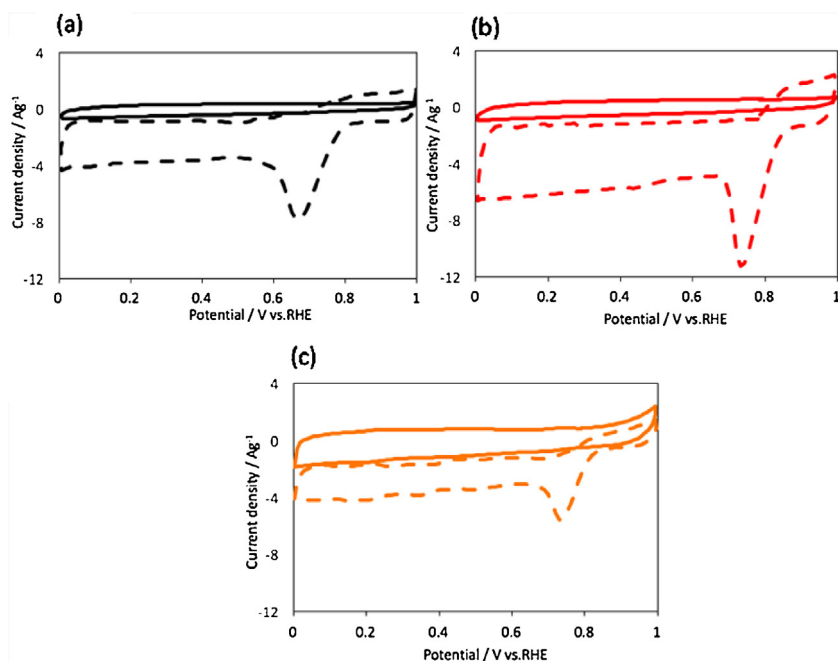


Fig. 3. Steady state voltammograms for (a) CNT, (b) CNT.Co.1%.500 and (c) CNT.Co.17%.500 catalysts in N_2 (solid line) and O_2 -saturated (dash line) 0.1 M KOH solution at 50mV/s respectively. Catalyst loading is 400 $\mu\text{g}/\text{cm}^2$.

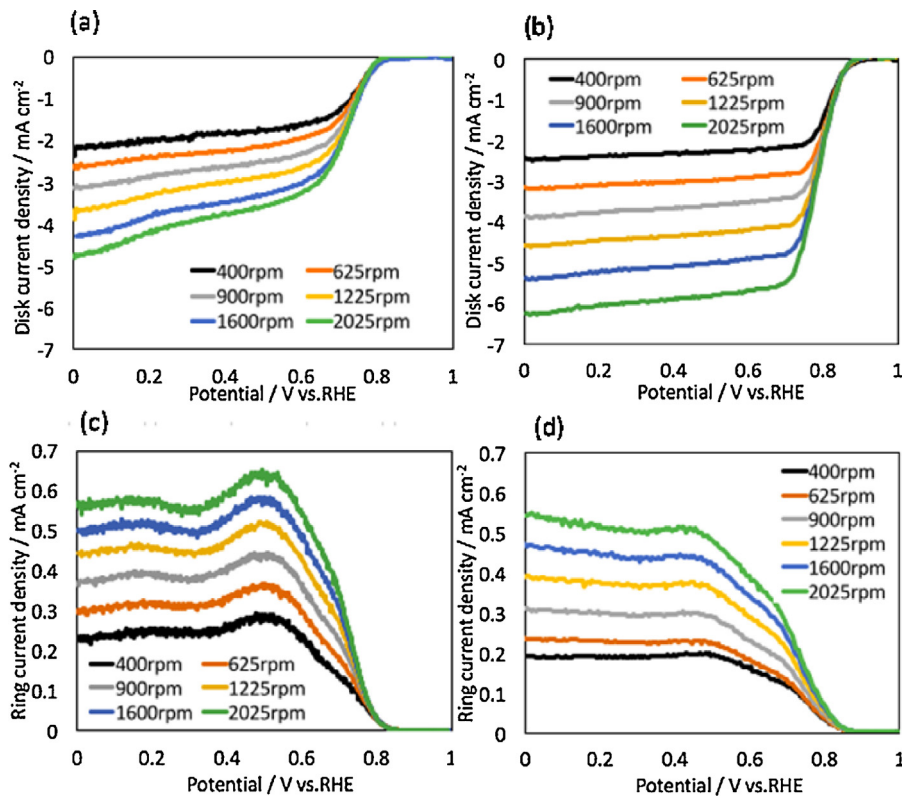


Fig. 4. LSVs during ORR for (a) CNT and (b) CNT_{Co}.1%_500 and ring currents divided by collection efficiency for the (c) CNT and (d) CNT_{Co}.1%_500 in O₂ – saturated 0.1 M KOH solution with a sweep rate of 5 mV/s respectively. Catalyst loading is 400 $\mu\text{g}/\text{cm}^2$.

by collection efficiency, 0.37) also increased with rotation rate as shown in Fig. 4. CNT_{Co}.1%_500 demonstrated lower ring current than CNT which indicates the formation of lower amount of hydrogen peroxide.

Fig. 5 presents the LSVs during ORR and electron transfer number (n) of the CNT, CNT_{Co}.1% (without heat treatment under N₂ at 500 °C), CNT_{Co}.1%_500 and Pt/Vulcan (20 wt.% Pt on Vulcan) catalysts measured at an electrode rotating rate of 1600 rpm with a potential scanning rate of 5 mV/s. The heat-treatment at 500 °C under N₂ was performed to remove the PVP from the catalysts [29]. As shown in Fig. 5, the catalyst without heat-treatment (CNT_{Co}.1%) has much lower LC and n than CNT. This is because the remaining PVP in the catalyst hinders the accessibility of oxygen to the active sites for ORR. However, the onset potential as well as LC of the CNT_{Co}.1%_500 were dramatically improved, while the selectivity of the reaction towards water formation was also enhanced. The CNT_{Co}.1%_500 reached LC of $-5.7 \text{ mA}/\text{cm}^2$ which is similar to that observed for Pt/Vulcan catalyst.

In order to clarify the influence of the PVP toward ORR activity, catalysts were also prepared without PVP (with Co precursor) or without Co precursor (with PVP). Fig. 6 presents the ORR currents for the CNT, CNT_{PVP}.500, CNT_{Co}.1%_noPVP_500 and CNT_{Co}.1%_500 measured at an electrode rotating rate of 1600 rpm with a potential scanning rate of 5 mV/s. The LC and n of the catalyst without PVP were higher than that of CNT. However, LC and n of CNT_{Co}.1%_noPVP_500 were not as much enhanced as CNT_{Co}.1%_500. Especially, LC of catalyst prepared without PVP showed a significantly lower value than that of CNT_{Co}.1%_500. Likewise, LC and n of the catalyst prepared without Co precursor (CNT_{PVP}.500) were not highly improved as CNT_{Co}.1%_500 showed, which implies that the effect of PVP toward ORR is negligible when the Co is not present on CNT.

These results reveal that PVP plays an important role during the synthesis of Co-containing catalyst, either favoring the formation of well dispersed NPs or introducing some electronic or chemical changes on the catalytic species. It is well known that PVP acts as a protecting agent of the colloidal particles preventing agglomeration. This has been manifested in different NPs composition like Pd nanoparticles and Sn-3.5Ag alloy NPs [29,38]. However, TEM images in Fig. 2 do not show relevant differences between both catalysts in terms of average particle size, suggesting that this is not the main factor explaining the effect of PVP.

On the other hand, as demonstrated in XPS N 1s in Fig. 1c and TEM image in Fig. 2f, PVP decomposition during catalyst pre-treatment produces a N-doped carbon shell on Co NP. Moreover, Fig. 1c shows that pyridinic-N and quaternary N groups are present on CNT_{Co}.1%_500. The presence of these Co-N-C species constitute active sites which facilitate the adsorption of oxygen, leading to improved ORR performance as it has been proposed by other authors [12,23]. It must be emphasized that when PVP is not used this carbon shell is not formed and N is not detected, which results in a lower activity of the Co-containing catalyst.

Different amounts of CoO_x NPs loaded on CNTs have been prepared to identify their effect on ORR activity. The ORR current densities and n of the catalysts with different Co contents (1, 9 and 17 wt.%) have been studied (Fig. S3 in Supplementary Data). The relationship between the Co content in the catalyst and LC as well as n at 0.3 V and 0.7 V (vs RHE) are summarized in Fig. 7. Remarkably, LC and n of the catalyst with 1 wt.% of CoO_x showed the highest values. As shown in Fig. 7a, the LC increased significantly up to a Co content of 1 wt.%, above which it decreased. The correlations of n and Co content in Fig. 7b presented similar behavior as LC. As displayed in Fig. 2, the average CoO_x NPs size follows the order of CNT_{Co}.17%_500 (12.3 nm) > CNT_{Co}.9%_500 (10.2 nm) > CNT_{Co}.1%_500 (8.5 nm). In contrast, LC and n follow the

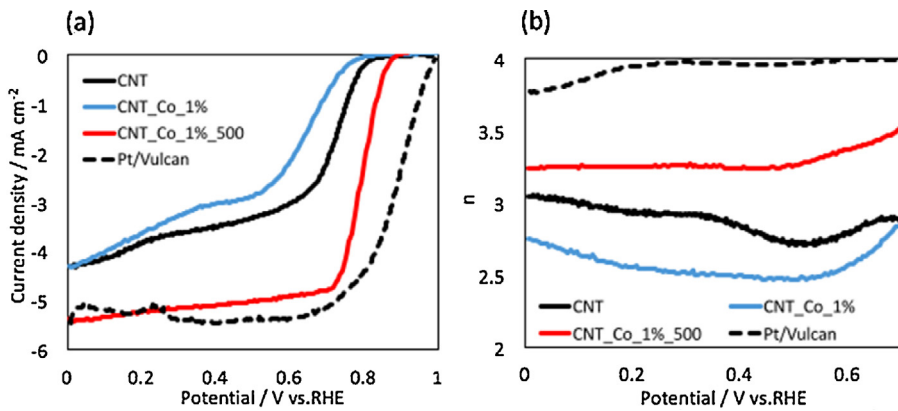


Fig. 5. (a) LSVs during ORR on the disk electrode and (b) electron transfer number (n) of the CNT, CNT.Co.1%, CNT.Co.1%.500 and Pt/Vulcan in O₂ – saturated 0.1 M KOH solution at 1600 rpm with a sweep rate of 5 mV/s respectively. Catalyst loading is 400 µg/cm².

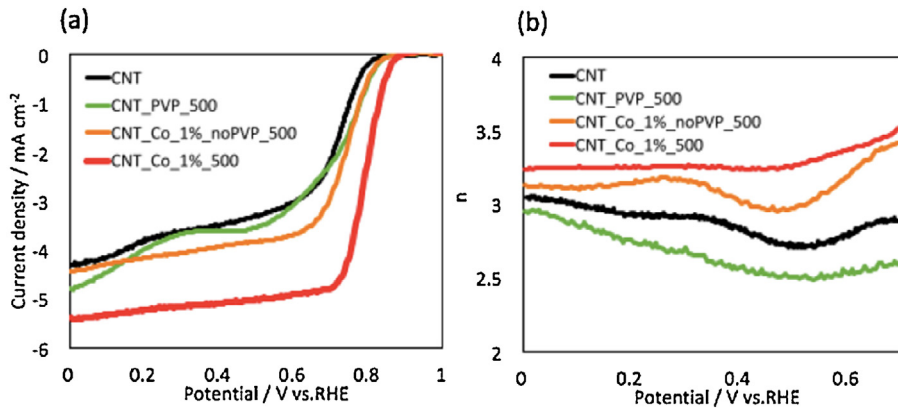


Fig. 6. (a) LSVs during ORR on the disk electrode and (b) n of the CNT, CNT_PVP_500, CNT_Co_1%.noPVP_500 and CNT_Co_1%.500 in O₂ – saturated 0.1 M KOH solution at 1600 rpm with a sweep rate of 5 mV/s respectively. Catalyst loading is 400 µg/cm².

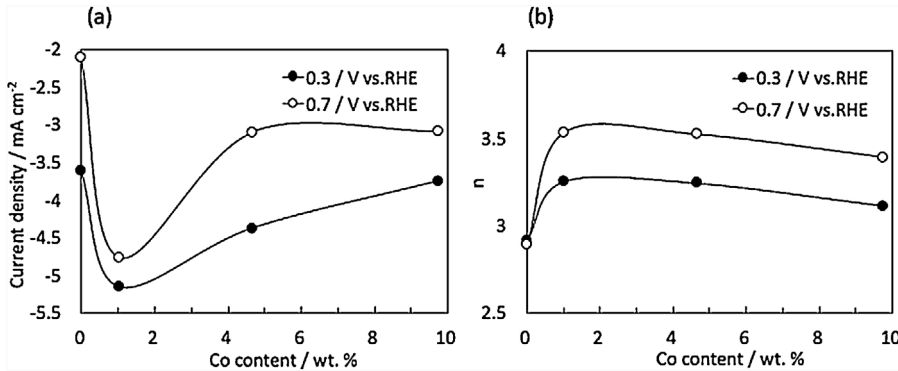


Fig. 7. Relationship between Co content and (a) LC as well as (b) n measured at 0.3 V and 0.7 V vs.RHE in O₂ – saturated 0.1 M KOH solution at 1600 rpm. Catalyst loading is 400 µg/cm². These catalysts were prepared with PVP and NaBH₄.

order CNT_Co_1%.500 > CNT_Co_9%.500 > CNT_Co_17%.500. In this sense, the results suggest that as the size of CoO_x NPs decreased, their ORR activities increased, which can be explained considering that ORR activity is enhanced by the smaller CoO_x NPs due to the enlarged interface between CoO_x and CNTs [24].

Though the LC of CNT_Co_1%.500 at 0.3 V (vs RHE) were similar to Pt/Vulcan (similar activity), the n value (~3.5) was lower than that of Pt/Vulcan (~4.0). It means that selectivity of CNT_Co_1%.500 is lower than Pt/Vulcan and follows a mix of a two and four electron pathway [26]. An associative pathway has been recently elucidated over CoO_x/C catalyst, which involves the following reactions: (i) O₂ + H₂O + 2e⁻ → HO₂⁻ + OH⁻; (ii) HO₂⁻ + H₂O + 2e⁻ → 3OH⁻ and

(iii) 2HO₂⁻ → O₂ + 2OH⁻. The interface between carbon and Co NPs can be identified as the most active sites for the first 2e⁻ reduction of oxygen to form HO₂⁻ [39]. Amount of active sites, which are responsible for reaction (i) in Co-containing catalysts, are larger than the amount of active sites for 4e⁻ electron pathway on Pt/Vulcan and thus, high LC for CNT_Co_1%.500 are obtained. In fact, the LC values are similar to Pt/Vulcan catalyst with a 20 wt.% of Pt in spite of the fact that the Co catalyst has only 1 wt.%. Thus, it might be explained that the first two electrons pathway reaction (i) O₂ + H₂O + 2e⁻ → HO₂⁻ + OH⁻ proceeds efficiently for CNT_Co_1%.500 due to their smaller Co NPs size which results in a

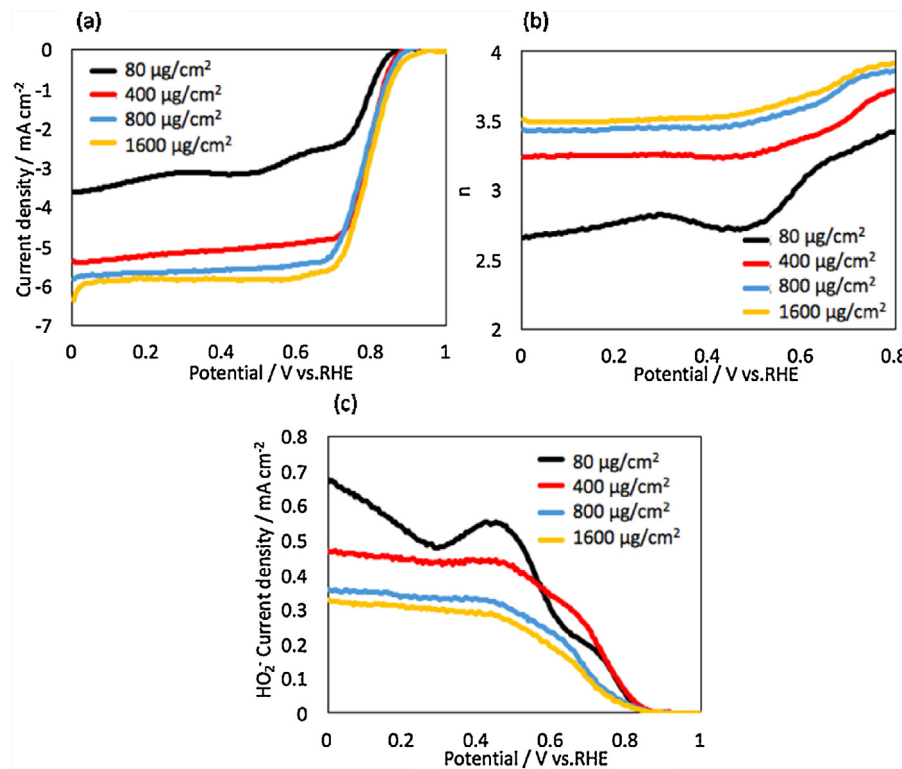


Fig. 8. (a) LSVs for ORR on the disk electrode, (b) n and (c) ring current of CNT_Co_1%_500 with different loadings in O₂ – saturated 0.1 M KOH solution at 1600 rpm with a sweep rate of 5 mV/s respectively.

larger interface between Co species and carbon producing a much higher amount of HO₂[–] [24].

In addition, Bonakdarpour et al. [40] reported that when the catalyst loading is low enough, the H₂O₂ molecules have a higher probability of diffusing away into the electrolyte than being reduced to water at a nearby site through reaction (ii). Therefore, the percentage of H₂O₂ released into the electrolyte strongly depends on the amount of electrocatalyst used on the RRDE [40]. Fig. 8 shows the ORR current densities and ring current densities as well as n for the CNT_Co_1%_500 measured for different loadings at rotation speed of 1600 rpm. At all potentials, the LC and n increased when larger loadings are used. At 1600 µg/cm², well defined mass transfer LC plateau of –6 mA/cm² as well as higher n (selectivity) was observed, probably indicating that close to four electrons are being generated for each oxygen molecule reaching the electrode through reaction (i) on the interface and (ii) HO₂[–] + H₂O + 2e[–] → 3OH[–] on the Co NPs surface [24]. As revealed in Fig. 8, the HO₂[–] yield decreased with increasing the loading (thickness) of the catalyst over the GC electrode. Additional experiments were designed to investigate about the effect of NaBH₄ towards ORR activity. Instead of NaBH₄, 1 wt.% of Co decorated catalysts synthesized with NH₃ were prepared. Two advantages for using NH₃ can be mentioned: first, the ammonia molecules tend to be strongly bonded to cobalt cations, working as a capping agent to hinder particle growth; second, the hydrolysis rate of cobalt salt can be well controlled by ammonia which releases hydroxyl ions [21,24]. Fig. 9 shows LSV curves for ORR and n for the catalysts prepared with and without NH₃. The LC of CNT_Co_1%_NH₃_500 is much lower than that of CNT_Co_1%_500. Fig. 2a and e show that the average CoOx NPs sizes of CNT_Co_1%_500 and CNT_Co_1%_NH₃_500 are about 8.5 nm. This means that Co NPs size of the catalysts prepared with NH₃ or NaBH₄ are very similar. It can be mentioned that not only Co NPs sizes but also the catalyst preparation procedure affects the ORR activity. According to the results of catalysts prepared herein, con-

tribution towards ORR activity of catalysts prepared using NaBH₄ was higher than that of NH₃.

The XPS results show three important differences among the two samples: (i) Fig. 1b suggests the presence of Co(II) and Co(III) for CNT_Co_1%_NH₃_500, probably forming Co₃O₄ species, when NaBH₄ is not used; (ii) metallic Co is observed when NaBH₄ is used and (iii) pyridinic-N and quaternary N groups improving ORR performance are present in all the catalysts prepared with NaBH₄ (see Fig. 1c and Table 2). Thus, it seems that the interaction of reduced Co with PVP is more efficient making that some Co-N species which work as active sites for ORR are formed after the heat treatment.

Dong et al. reported that Co²⁺ ions coordinated with NH₃ form [Co(NH₃)₆]²⁺ ions and most of them were immediately oxidized to [Co(NH₃)₆]³⁺ by O₂ according to the reaction 4[Co(NH₃)₆]²⁺ + O₂ + 2H₂O = 4[Co(NH₃)₆]³⁺ + 4OH[–]; then, after heat treatment Co₃O₄ nanomaterials are obtained [41]. Therefore Co(III) could be detected on CNT_Co_1%_NH₃_500. Liang et al. suggested that the carbon hybrid materials prepared with CoO contain larger amount of effective active or accessible ORR active sites than the carbon hybrid materials containing Co₃O₄ [25]. Furthermore, Xiao et al. investigated the relationship between surface structure of various types of cobalt oxide nanoparticles and their ORR activities [42]. It was concluded that the catalytically active sites for ORR should be the surface tetrahedral Co(II) sites.

Regarding metallic Co, it must be mentioned that Co(II) or Co(III) cannot be reduced in absence of NaBH₄. Actually, Co metallic was not found in other catalysts prepared with NH₃ which is in agreement with our results [21,22]. Wang et al. showed that in the catalysts with N-doped reduced graphene oxide aerogel (NGA), CoO and Co (CoO/Co-NGA) subunits had higher ORR activity than the catalysts without Co metallic (CoO-NGA) composites [43]. Highly integrated NGA, CoO and Co, suggests strong bonding between them, which would enhance the interaction between the metal oxide NPs and the graphene support, promoting electron

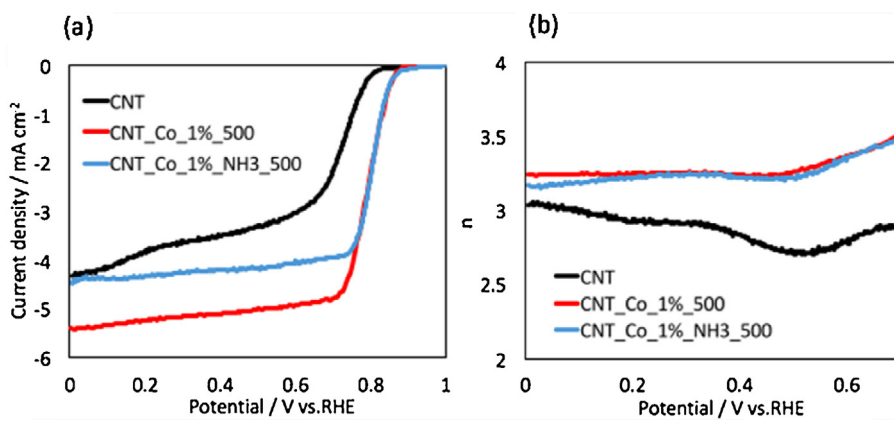


Fig. 9. (a) LSVs during ORR on the disk electrode and (b) n of the CNT, CNT.Co.1%.500 and CNT.Co.1%.NH3.500 in O₂ – saturated 0.1 M KOH solution at 1600 rpm with a sweep rate of 5 mV/s respectively. Catalyst loading is 400 $\mu\text{g}/\text{cm}^2$.

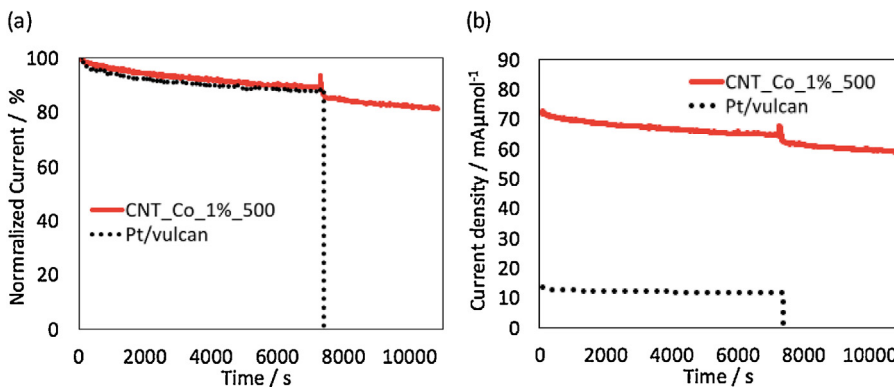


Fig. 10. Current versus time for CNT.Co.1%.500 and Pt/Vulcan at 0.65 V vs. RHE in O₂ – saturated 0.1 M KOH solution at 1600 rpm referred to (a) disk electrode area on normalized current base and (b) mol of Co or Pt in the catalyst. Catalyst loading is 400 $\mu\text{g}/\text{cm}^2$.

and charge transfer among the active sites. Finally, the presence of Co-pyridinic-N and quaternary N groups, formed through the interaction of PVP and Co during the NPs synthesis when NaBH₄ is used, result in higher catalytic activity species as indicated by other authors [12,23].

In summary, different factors contribute to the optimum catalytic activity of Co NPs supported on nanostructured carbons. On the one hand, particle size has an important role since lower particle size results in larger amount of Co-Carbon interface sites. On the other hand, the Co-species composition has an important contribution since the presence of lower oxidation state Co sites and Co-N species results in enhanced catalytic activity when comparing catalysts with similar particle size.

3.3. Durability tests

The durability of an ORR catalyst is a factor which determines the life of a fuel cell [9]. The stability of the Co-containing catalyst was measured by RDE chronoamperometry under steady state mass transport conditions (0.65 V vs RHE). Fig. 10 shows the stability of the CNT.Co.1%.500 and Pt/Vulcan catalysts on normalized current base. The current density calculated on Co and Pt content in molar basis is also included in Fig. 10. Additionally, methanol poisoning test was performed by adding 1 M methanol into the electrolyte after 2 h reaction [31]. As shown in Fig. 10, even after adding methanol, CNT.Co.1%.500 catalyst activity is more than 80% of the initial value over 3 h. However, the current of the Pt/vulcan dropped to zero immediately after addition of methanol. The experiment supports that the Co-containing catalysts are suitable in

terms of stability and resistance towards methanol. Furthermore, the current of CNT.Co.1%.500 per mole of metal content is higher than for Pt/Vulcan, showing that it is possible to achieve higher current densities than for Pt based catalysts with very low amounts of CoO_x (i.e., 1 wt.% in this study). In addition, potential cycling durability tests were carried out by cyclic voltammetry. The cycling was repeated under O₂-saturated 0.1 M KOH solution at 50 mV s⁻¹ from 0 to 1 V (vs.RHE) for 500 cycles. Fig. 11 presents the LSV curves before and after the 500 cycling (LSV curve after 100 cycles is indicated only for CNT.Co.1%.500). As demonstrated in Fig. 11, the half-wave potential for CNT.Co.1%.500 and Pt/Vulcan catalysts shifted to lower potentials by only 5 mV and 15 mV after 500 cycles, respectively. These results imply that our catalysts show good stability in alkaline solution which means that they are interesting as catalysts for alkaline fuel cells.

4. Conclusions

A facile method to synthesize Co NPs decorated CNTs catalysts which show efficient and stable activity for ORR was developed. Our catalyst containing 1 wt.% of Co NPs (average NPs: 8.5 nm) prepared with PVP as protecting agent and NaBH₄ has surprisingly high LC in alkaline solution which is similar to commercial Pt/Vulcan. The catalyst showed higher selectivity towards 4e⁻ electron pathway than CNT. Higher ORR activity is possible for smaller size of Co NPs catalysts due to the enlarged interfaces between Co species and CNTs. The addition of PVP and NaBH₄ during the preparation procedure is necessary for obtaining the highest activity since it favors the formation of lower oxidation states for Co species and the formation of

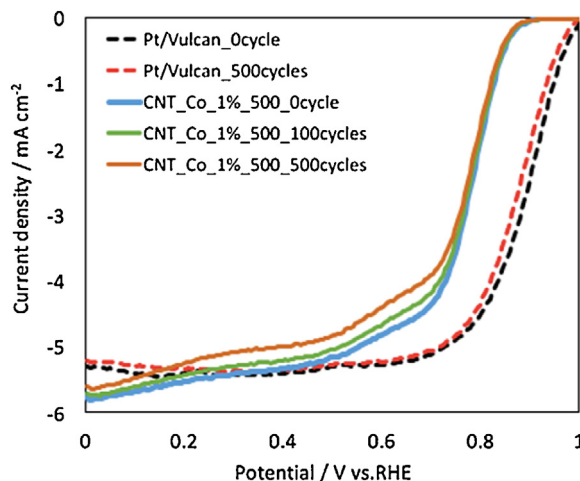


Fig. 11. LSV curves for CNT.Co.1%_500 and Pt/Vulcan before and after the cycling, in O_2 – saturated 0.1 M KOH solution at 1600 rpm with a sweep rate of 5 mV/s. Catalyst loading is 400 $\mu\text{g}/\text{cm}^2$.

a N-doped carbon shell. The Co-containing catalysts with small particle sizes, low Co oxidation states and pyridinic N and quaternary N groups in the carbon framework seem to have the optimum combination to create the most active sites for this reaction. These results suggest that the synthesis of smaller particle sizes than those used in this study (below 8 nm) employing this preparation method can produce improved Co-based ORR catalysts and that this methodology could also be applied to other metal oxides to achieve improved ORR catalysts.

Acknowledgments

The authors would like to thank GV and FEDER (PROMETEOII/2014/010), projects CTQ2015-66080-R (MINECO/FEDER), MAT2016-76595-R (MINECO/FEDER), BES-2013-063678 and HEIWA NAKAJIMA FOUNDATION for the financial support.

Appendix A. Supplementary data

Supplementary data associated with this article can be found, in the online version, at <http://dx.doi.org/10.1016/j.apcatb.2017.05.096>.

References

- [1] C. Lamy, Carbons electrochem, in: E.F. François Beigui (Ed.), *Energy Storage Convers. Syst.*, CRC Press, 2010, pp. 377–410.
- [2] M. Winter, R.J. Brodd, *Chem. Rev.* 104 (2004) 4245–4270.
- [3] F. Bidault, D.J.L. Brett, P.H. Middleton, N.P. Brandon, *J. Power Sources* 187 (2009) 39–48.
- [4] N. Daems, X. Sheng, I.F.J. Vankelecom, P.P. Pescarmona, *J. Mater. Chem. A* 2 (2014) 4085–4110.
- [5] Z. Yang, H. Nie, X. Chen, X. Chen, S. Huang, *J. Power Sources* 236 (2013) 238–249.
- [6] K. Gong, F. Du, Z. Xia, M. Durstock, L. Dai, *Science* 323 (2009) 760–764.
- [7] G. McLean, *Int. J. Hydrogen Energy* 27 (2002) 507–526.
- [8] P. Trogadas, T.F. Fuller, P. Strasser, *Carbon* 75 (2014) 5–42.
- [9] B. You, P. Yin, J. Zhang, D. He, G. Chen, F. Kang, H. Wang, Z. Deng, Y. Li, *Sci. Rep.* 5 (2015) 11739.
- [10] G. Zhang, W. Lu, F. Cao, Z. Xiao, X. Zheng, *J. Power Sources* 302 (2016) 114–125.
- [11] A. Pendashteh, J. Palma, M. Anderson, R. Marcilla, *Appl. Catal. B Environ.* 201 (2017) 241–252.
- [12] T. Sun, L. Xu, S. Li, W. Chai, Y. Huang, Y. Yan, J. Chen, *Appl. Catal. B Environ.* 193 (2016) 1–8.
- [13] P.W. Menezes, A. Indra, D. González-Flores, N.R. Sahraie, I. Zaharieva, M. Schwarze, P. Strasser, H. Dau, M. Driess, *ACS Catal.* 5 (2015) 2017–2027.
- [14] Y. Liang, Y. Li, H. Wang, H. Dai, *J. Am. Chem. Soc.* 135 (2013) 2013–2036.
- [15] C.H. Choi, M.W. Chung, H.C. Kwon, J.H. Chung, S.I. Woo, *Appl. Catal. B Environ.* 144 (2014) 760–766.
- [16] S. Zhao, B. Rasimick, W. Mustain, H. Xu, *Appl. Catal. B Environ.* 203 (2017) 138–145.
- [17] G. Wu, K.L. More, C.M. Johnston, P. Zelenay, *Science* 332 (2011) 443–447.
- [18] M. Wang, J. Huang, M. Wang, D. Zhang, W. Zhang, W. Li, J. Chen, *Electrochem. Commun.* 34 (2013) 299–303.
- [19] J. Xu, P. Gao, T.S. Zhao, *Energy Environ. Sci.* 5 (2012) 5333–5339.
- [20] S. Chao, W. Guo, *Anal. Sci.* 29 (2013) 619–623.
- [21] Y. Liang, Y. Li, H. Wang, J. Zhou, J. Wang, T. Regier, H. Dai, *Nat. Mater.* 10 (2011) 780–786.
- [22] Q. He, Q. Li, S. Khene, X. Ren, F.E. López-Suárez, D. Lozano-Castelló, A. Bueno-López, G. Wu, *J. Phys. Chem. C* 117 (2013) 8697–8707.
- [23] X. Yuan, L. Li, Z. Ma, X. Yu, X. Wen, Z.-F. Ma, L. Zhang, D.P. Wilkinson, J. Zhang, *Sci. Rep.* 6 (2016) 20005.
- [24] J. Liu, L. Jiang, B. Zhang, J. Jin, D.S. Su, S. Wang, G. Sun, *ACS Catal.* 4 (2014) 2998–3001.
- [25] Y. Liang, H. Wang, P. Diao, W. Chang, G. Hong, Y. Li, M. Gong, L. Xie, J. Zhou, J. Wang, T.Z. Regier, F. Wei, H. Dai, *J. Am. Chem. Soc.* 134 (2012) 15849–15857.
- [26] L.M. Uhlig, G. Sievers, V. Brüser, A. Dyck, G. Wittstock, *Sci. Bull.* 61 (2016) 612–618.
- [27] Y. Li, W. Zhou, H. Wang, L. Xie, Y. Liang, F. Wei, J.-C. Idrobo, S.J. Pennycook, H. Dai, *Nat. Nanotechnol.* 7 (2012) 394–400.
- [28] C.W.B. Bezerra, L. Zhang, K. Lee, H. Liu, A.L.B. Marques, E.P. Marques, H. Wang, J. Zhang, *Electrochim. Acta* 53 (2008) 4937–4951.
- [29] I. Miguel-García, A. Berenguer-Murcia, T. García, D. Cazorla-Amorós, *Catal. Today* 187 (2012) 2–9.
- [30] U.A. Paulus, T.J. Schmidt, H.A. Gasteiger, R.J. Behm, *J. Electroanal. Chem.* 495 (2001) 134–145.
- [31] Y. Huang, M. Zhang, P. Liu, L. Wang, F. Cheng, *Ionics* 22 (2016) 1425–1432.
- [32] D. Barreca, C. Massignan, S. Daolio, M. Fabrizio, C. Piccirillo, L. Armelao, E. Tondello, *Chem. Mater.* 13 (2001) 588–593.
- [33] K. Niu, B. Yang, J. Cui, J. Jin, X. Fu, Q. Zhao, J. Zhang, *J. Power Sources* 243 (2013) 65–71.
- [34] P. Bazylewski, D.W. Boukhvalov, A.I. Kukharenko, E.Z. Kurmaev, A. Hunt, A. Moewes, Y.H. Lee, S.O. Cholakh, G.S. Chang, *RSC Adv.* 5 (2015) 75600–75606.
- [35] E.E. Raymundo-Pinero, D. Cazorla-Amorós, A. Linares-Solano, J. Find, U. Wild, R. Schlogl, *Carbon* 40 (2002) 597–608.
- [36] E. Raymundo-Pinero, D. Cazorla-Amorós, A. Linares-Solano, *Carbon* 41 (2003) 1925–1932.
- [37] I.G. Casella, M. Contursi, *J. Solid State Electrochem.* 16 (2012) 3739–3746.
- [38] H.J. Pan, C.Y. Lin, U.S. Mohanty, J.H. Chou, *Mater. Sci. Appl.* 2 (2011) 1480–1484.
- [39] J. Liu, L. Jiang, Q. Tang, B. Zhang, D.S. Su, S. Wang, G. Sun, *ChemSusChem* 5 (2012) 2315–2318.
- [40] A. Bonakdarpour, M. Lefevre, R. Yang, F. Jaouen, T. Dahn, J.-P. Dodelet, J.R. Dahn, *Electrochim. Solid-State Lett.* 11 (2008) B105–B108.
- [41] Y. Dong, K. He, L. Yin, A. Zhang, *Nanotechnology* 18 (2007) 435602–435608.
- [42] J. Xiao, Q. Kuang, S. Yang, F. Xiao, S. Wang, L. Guo, *Sci. Rep.* 3 (2013) 2300–2307.
- [43] M. Wang, Y. Hou, R.C.T. Slade, J. Wang, D. Shi, D. Wexler, H. Liu, J. Chen, *Front. Chem.* 4 (2016) 1–10.